Research Article ISSN 2689-1050

Chemical & Pharmaceutical Research

Crystallographic, DFT, Lattice Energy and Hirshfeld Surface Analysis of Some CSD-Based 6-Chloropurines

Jigmat Stondus and Rajni Kant*

Chemical Crystallography Laboratory, Department of Physics, University of Jammu, Jammu, India.

***Correspondence:**
Chemical Crystallography Laboratory, Department of Physics, University of Jammu, Jammu Tawi-180006, India, Tel:+91 9419194375, Fax: +91 191 243 2051.

Received: 02 May 2022; **Accepted:** 23 May 2022; **Published:** 02 June 2022

Citation: Stondus J, Kant R. Crystallographic, DFT, Lattice Energy and Hirshfeld Surface Analysis of Some CSD-Based 6-Chloropurines. Chem Pharm Res. 2022; 4(2): 1-14.

ABSTRACT

A comparative crystallographic and detailed computational analysis of four known 6-chloropurine X-ray structures, accessed from the CSD repository, has been reported in this paper. The quantum chemical analysis of each structure, including the optimized geometry, lattice energy, Hirshfeld surface, HOMO-LUMO energies, has been made to account for the properties of this class of biologically important organic materials. The lattice energy contribution in terms of intermolecular interactions, responsible for the packing stability, has been estimated by PIXEL procedure. Three-dimensional Hirshfeld surfaces and the corresponding 2D-fingerprint plots include the analysis of short intermolecular contacts. The π…π interactions and stacking features of molecules in the packing, have been analyzed using shape index and curvedness plots.

Keywords

Chloropurines, DFT, Lattice energy, PIXEL method, Hirshfeld surface analysis.

Introduction

Purine is water-soluble, nitrogen containing heterocyclic organic compound consist of two rings (pyrimidine and imidazole rings). Nitrogen containing heterocyclic compounds are one of the most essential structural components in pharmaceutical products. As per the database of FDA-approved medications in the United States, nitrogen heterocycles are found in sixty percent of small-molecule therapies [1]. Purine derivatives, such as *adenine* and *guanine* found in DNA and involves in stabilizing the two strands of DNA helix by forming hydrogen bonds [2]. Purine-based molecules have proven to be highly effective kinase inhibitors [3,4], possesses antitumor activity [5], antiviral activity against vaccinia virus [6]. Many of the biologically active compounds, including many commonly used drugs, have been discovered through the structural modification of purine bases, nucleosides, and nucleotides [7]. Synthesis and biological activities of purine and its derivatives have been reviewed from time to time [8-11].

X-ray crystallography is being used extensively in structure-based drug design, and complete characterization of target macromolecules and macromolecule-ligand complexes is required at all stages [12]. Therefore, the role of computational quantum chemistry is also becoming extremely valuable in the domains of biochemical and materials science [13]. In organic chemistry, it aids in the knowledge to look deeper into the reaction mechanisms, through the assessment of geometrical features of the molecules [14,15]. A wide range of organic problems has been solved because of the strengthening connections between experimental and computational chemistry [16]. In this context, the present study is aimed to perform some theoretical analysis of the crystal structures of few chloro-purine structures, whose experimental X-ray diffraction analyses have already been reported [17-19]. The purine nucleus and chemical structures of chloro-purines retrieved from the Cambridge structure database are presented in Figure 1. A comprehensive analysis of the interaction energies of various intermolecular interactions in the crystal packing with special emphasis on the role of substituted chlorine atoms in packing shall be presented in detail.

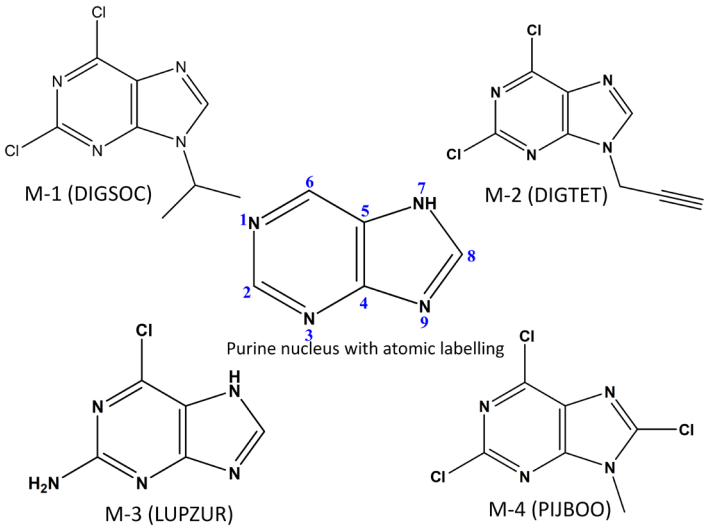

Figure 1: Chemical structure of purine nucleus and 6-chloro-purine derivatives.

Computational Procedures

DFT Calculations

Density functional theory (DFT) is a quantum chemical modeling method used to explore the electronic structures of many body systems, based on calculating the total electron densities. It has gain popularity in modern day's calculation due to lower computation cost as compared to traditional *ab-initio* methods [20]. *DFT* calculations were performed on the Cl-substituted purine structures, by using their CIF files to supply the atomic coordinates in Gaussian 09 software package [21]. The ground state molecular geometry optimization was performed at B3LYP/6-311+G (d,p) level [22,23] with no symmetry constraints and, the Gassview 6.0.16 software is employed to for visual analysis [24]. The optimized structure parameters (such as bond distances and bond angles) were compared with the experimentally determined corresponding values. Using the optimized structural parameters, molecular orbital analysis for highest occupied molecular orbital (HOMO) and lowest unoccupied molecular orbital (LUMO) were carried out and subsequently determined the global reactivity parameters for each structures.

PIXEL energy calculation

The lattice energies and the intermolecular interaction energies calculation of the molecules were carried out by PIXEL program [25]. Pixel method is a semi-empirical approach to calculate the intermolecular interaction energy between molecular pairs and thereby the lattice energy, of the crystal structures by considering electron densities of the atoms as pixels [26]. The PIXEL energy calculation is based on the tom-atom Coulomb-London-Pauli model which enables to calculate the interaction potential energies into different components, namely Coulombic, Polarization, dispersion and repulsion [27]. The electron densities required for the calculation of pixel energy is obtained by Gussian 09 using MP2/6-31G** basis set [21].

Hirshfeld Surface Analysis

The Hirshfeld surface is a visual representation tool used for identifying various intermolecular interactions present in the crystal structure of a molecule and is powerful method to quantify the role of each interaction in packing stability [28,29]. Hirshfeld surfaces of all the molecules (M-1 to M-4) were generated by using the CIF files as input in the latest CrystalExplorer software package [v-21.5] [30]. The d_{norm} plots, shape index plots, curvedness plots and 2D fingerprint plots were used for visualizing and quantify the role of each intermolecular contact in determining packing features.

Results and Discussion

Crystallographic comparison

The precise crystal data for each structure as mined from the database is presented in Table 1. The crystal structures have been reported with a reasonably low value of the reliability index (R-factor) [4.86% (M-1), 4.38% (M-2), 3.84% (M-3) and 3.31% (M-4)]. A comparison of the experimental bond distances and angles of the central purine ring-system (Figure 2) shows that the bond lengths and bond angles within the limits of experimental errors and no significant deviation has been observed.

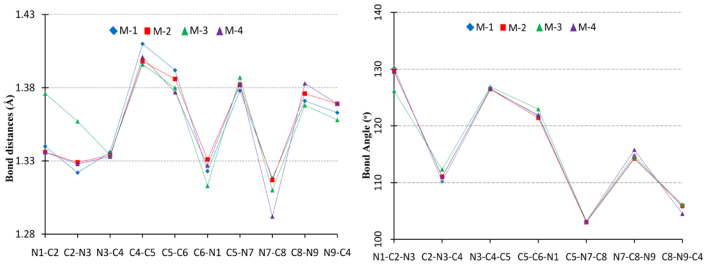

Figure 2: Comparison of bond distances and angles of central purine ring-system (M-1 to M-4).

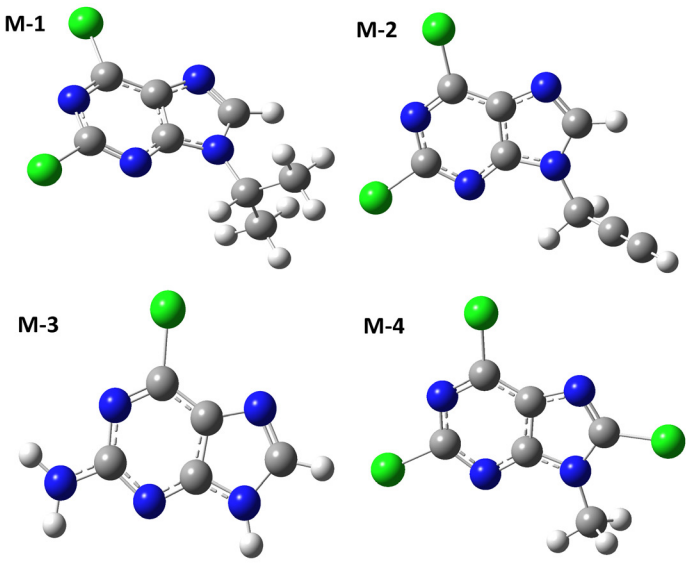

Figure 3: DFT optimized structures (M-1 to M-4).

Table 1: Precise crystal data for the CSD structures.

Identification code	M-1	M-2	M-3	M-4
CCDC code	DIGSOC	DIGTET	LUPZUR	PIJBOO
Empirical formula	$C_8H_8Cl_2N_4$	$C_8H_4Cl_2N_4$	$C_5H_4ClN_5$	$C_6H_3C1_3N_4$
Formula weight	231.08	227.05	169.58	237.5
Temperature/K	293(2)	293(2)	150(2)	235
Crystal system	monoclinic	monoclinic	tetragonal	triclinic
Space group	$P2_1/c$	$P2_1/n$	$P4_12_12$	P-1
a/Å b/Å c/Å	8.4703(10) 17.6304(19) 6.9442(7)	3.9928(3) 20.7240(14) 11.2562(8)	7.0855(10) 7.0855(10) 26.990(5)	7.334(2) 7.568(2) 9.146(2)
α/°, β/°, γ/°	90, 102.628, 90	90, 98.97, 90	90, 90, 90	106.3, 90.2,115.6
Volume/Å^3	1011.93(19)	920.01(11)	1355.0(4)	434.612
Z	4	4	8	2
ρ_{calc}g/cm^3	1.517	1.639	1.663	1.815
Radiation MoK_α	λ = 0.71073	λ = 0.71073	λ = 0.71073	λ = 0.71073
Final R-Factor	4.86	4.38	3.84	3.31

Table 2: Comparison of experimental and theoretical geometrical parameters.

Atoms	M-1		M-2		M-3		M-4	
	XRD	DFT	XRD	DFT	XRD	DFT	XRD	DFT.
	Bond Distance (Å)							
N1-C2	1.340	1.338	1.336	1.333	1.376	1.357	1.336	1.332
C2-N3	1.322	1.322	1.329	1.324	1.357	1.342	1.328	1.325
N3-C4	1.336	1.330	1.334	1.328	1.334	1.326	1.333	1.326
C4-C5	1.410	1.412	1.398	1.410	1.396	1.410	1.401	1.410
C5-C6	1.392	1.394	1.386	1.394	1.380	1.395	1.377	1.394
C6-N1	1.323	1.322	1.331	1.322	1.313	1.313	1.327	1.321
C5-N7	1.378	1.376	1.382	1.378	1.387	1.384	1.383	1.378
N7-C8	1.318	1.309	1.317	1.306	1.310	1.302	1.292	1.298
C8-N9	1.371	1.382	1.376	1.384	1.368	1.387	1.383	1.384
N9-C4	1.363	1.372	1.369	1.372	1.358	1.372	1.369	1.374
C2-Cl1	1.730	1.738	1.713	1.748	1.736	1.746	1.722	1.738
	Bond Angle (°)							
N1-C2-N3	130.27	128.48	129.64	128.32	126.18	126.67	129.57	128.43
C2-N3-C4	110.19	112.10	111.06	111.98	112.34	112.43	111.00	111.88
N3-C4-C5	126.42	126.16	126.48	126.52	126.90	126.96	126.54	126.50
C5-C6-N1	121.92	120.92	121.41	120.84	122.95	121.58	121.77	120.77
C5-N7-C8	103.13	104.07	103.03	104.30	103.21	104.45	103.16	103.57
N7-C8-N9	114.78	114.49	114.22	114.06	114.34	113.44	115.77	115.45
C8-N9-C4	105.73	105.28	105.91	105.70	106.17	106.62	104.50	104.60

Structure Optimization

The DFT optimized geometrical structures of all the four Cl-substituted purine derivatives are presented in Figure 3. A comparison of X-ray determined bond distances and bond angles has been made with the DFT calculated data (Table 2). The theoretically calculated bond distances show insignificant variation vis-à-vis X-ray data. Among all the structure, the maximum difference found in bond distances is ~ 0.019Å [observed in case of N1-C2 and C8-N9 bonds (M-3)].

In order to emphasize the relationship between theoretical (DFT) and experimental (XRD) geometrical parameters, the correlation coefficients (R^2) of bond distances and bond angles of the purine nucleus were calculated and the results show that the R^2 values are close to 1, an indication for the existence of a strong correlation between the experimental and the theoretical values. Correlation plots for the bond distances and bond angles of all the four molecules are presented in Figure 4.

Frontier Molecular Orbital Analysis

Chemical characteristics of the molecules are significantly influenced by the HOMO-LUMO orbitals [31] generated for each molecule by using DFT/B3LYP/6311-G+(d,p) and the pictorial representation of these orbitals is presented in Figure 5. The HOMO-LUMO orbitals are localized to the central ring system and the chlorine substituent, in case of M-1, M-2 and M-4, whereas it is delocalized over the whole molecule in M-3. The HOMO-LUMO energy gap (ΔE) is a parameter that defines the ultimate charge transfer interaction within the molecule [32]. By and large, its value in case of M-1, M-2 and M-4 is the same while it is relatively small in case of M-3. This could probably be attributed to the formation of a C=N bond by the primary amino

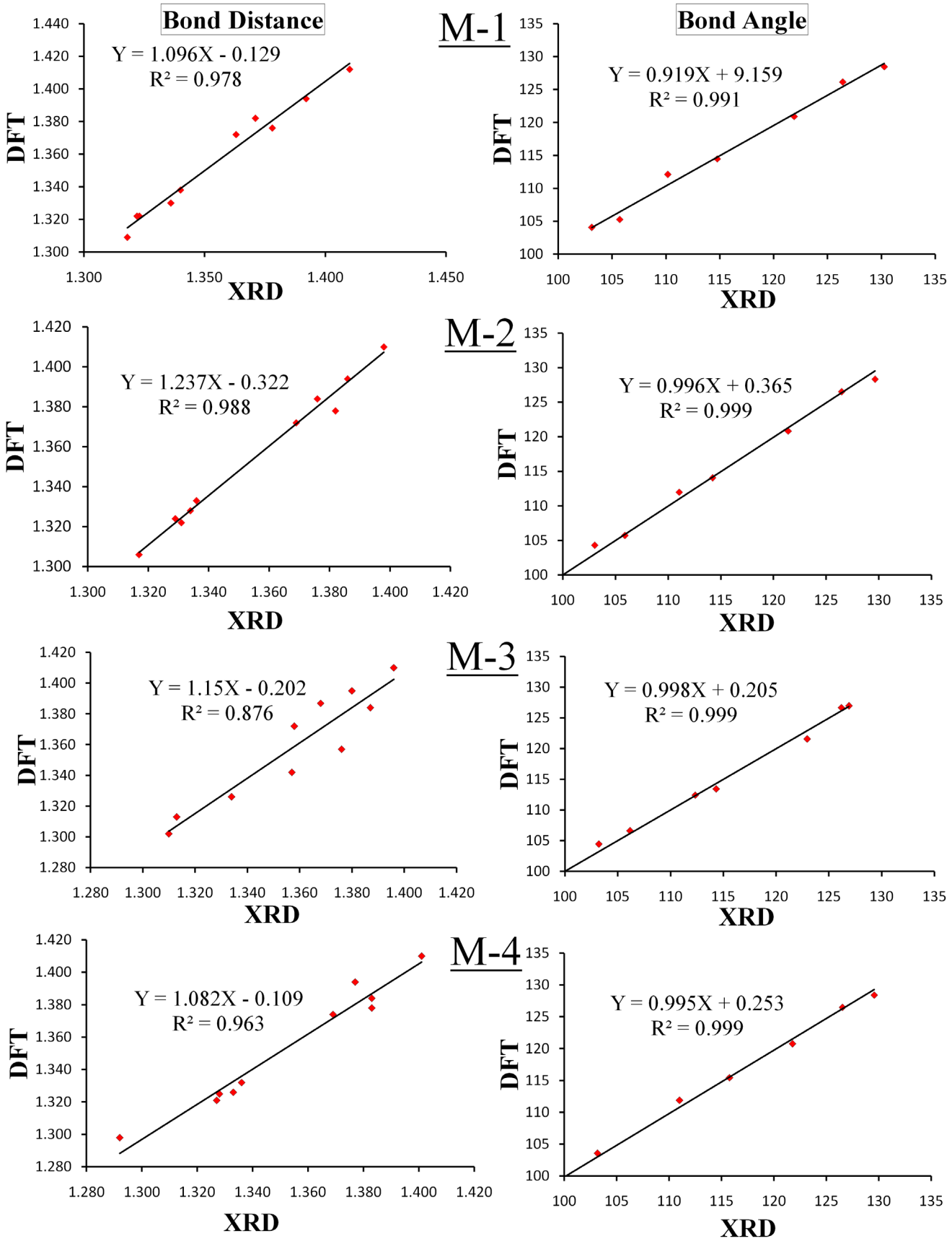

Figure 4: Experimental (XRD) vs. theoretical (DFT) bond distance and bond angle correlation plots.

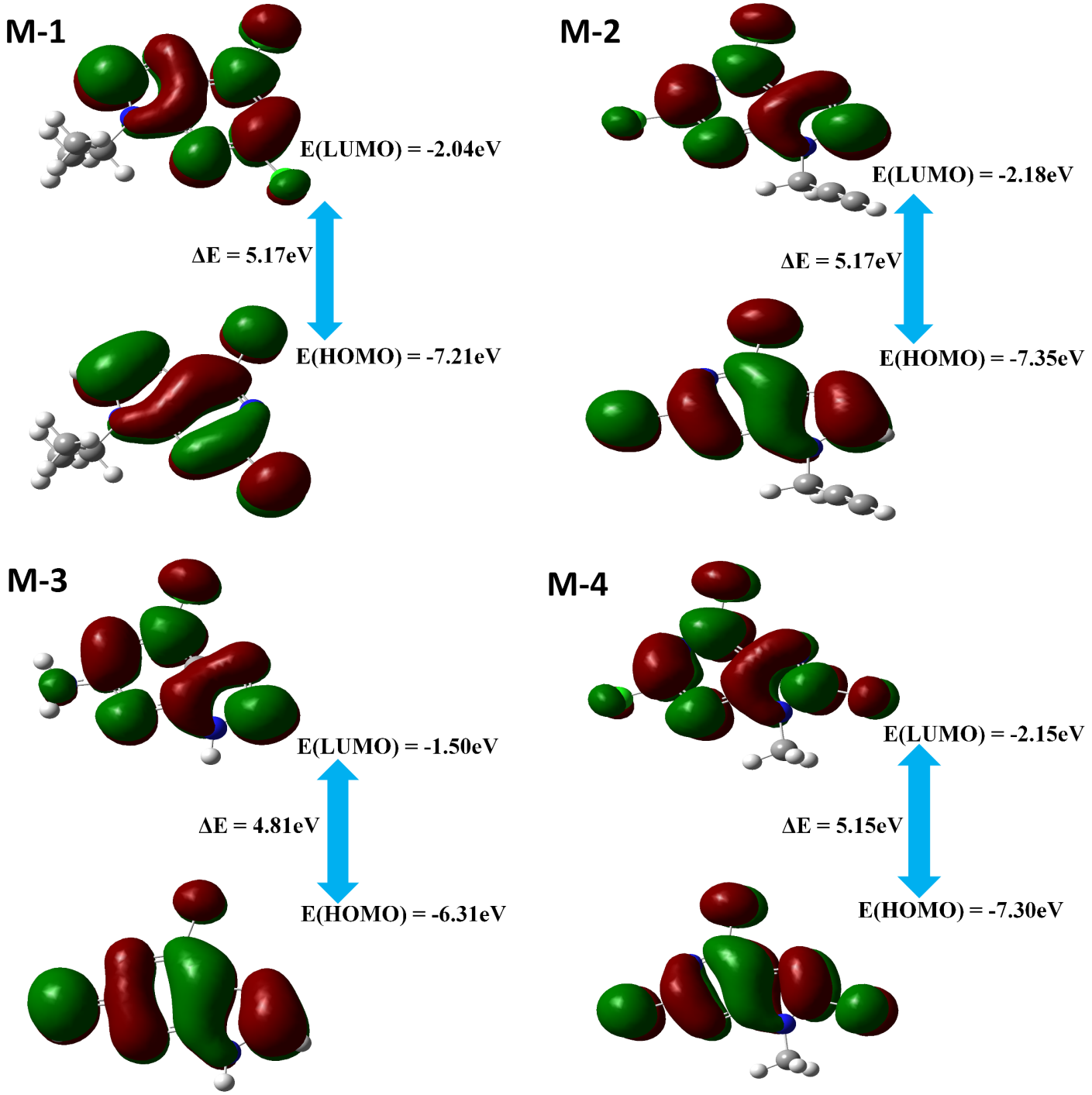

Figure 5: HOMO-LUMO energies in the molecules.

group attached at C2 [33]. HOMO-LUMO energies were further used to calculate various chemical properties of the molecule which are termed as global reactivity parameters (Table 3).

The HOMO- LUMO energies and its derived parameters such as chemical hardness, chemical softness, etc. explains much about the chemical reactivity and stability of the molecules [34,35]. The ΔE and chemical hardness values indicate that the structure M-1 and M-2 are most stable as compared to M-3 and M-4 [36]. Electrophilicity index and electronegativity of the structures follows the order as M-2>M-4>M-1>M-3; indicating that M-2 and M-3 are best electrophile and nucleophile, respectively.

Lattice energy and Intermolecular Interaction Energy Analysis

Table 4 contains the lattice energies calculated for each structure and the total lattice energy (E_{Tot}) of the structures lies in the range, -28 to -38 kcal/mol. The total lattice energy in case of M-3 is relatively large as compared to the remaining structures. The

Table 3: Global reactivity parameters of the molecules.

Parameters	M-1	M-2	M-3	M-4
E(HOMO) (eV)	-7.21	-7.35	-6.31	-7.30
E(LUMO) (eV)	-2.04	-2.18	-1.50	-2.15
ΔE=[E(LUMO) - E(HOMO)] (eV)	5.17	5.17	4.81	5.15
Chemical Hardness, η = ΔE/2 (eV)	2.585	2.585	2.405	2.575
Softness, ζ = ½ η (eV)	0.1934	0.1934	0.2079	0.1942
Chemical Potential, (μ = [E(LUMO) + E(HOMO)]/2) (eV)	-4.625	-4.765	-3.905	-4.725
Electrophilicity Index, ω = $\mu^2/2\eta$ (eV)	4.137	4.392	3.170	4.335
Electronegativity, χ = - μ (eV)	4.625	4.765	3.905	4.725

Table 4: Lattice energy calculated for M-1, M-2, M-3 and M-4

Molecule	E_{Cou}	E_{Pol}	E_{Dis}	E_{Rep}	E_{Tot}
M-1	-10.445	-4.063	-32.959	18.571	-28.920
M-2	-13.743	-5.091	-32.935	20.722	-31.047
M-3	-31.979	-14.412	-30.473	39.388	-37.476
M-4	-11.018	-4.398	-36.448	23.757	-28.083

energy components of M-1, M-2 and M-4 in Table 4 shows that the dispersion energy has dominant role to play in the stability of molecular packing (around 63-70% contribution), whereas the coulomb energy in case of M-3 is less dominant, possibly due to the existence of strong N-H…N hydrogen bonding interactions. A precise description of results as obtained from the *PIXEL* calculation in respect of each molecule is mentioned below:

M-1. 2, 6-Dichloro-9-isopropyl-9H-purine

The molecular pairs (1-6) involved in the crystal packing of 2, 6-Dichloro-9-isopropyl-9H-purine with associated interaction energies are presented in Figure 6. The π…π stacking interactions along with C-H…Cl and C-H…N hydrogen bonds, forms the most stable interaction pair (motif-1) with interaction energy (I.E.) = -11.337 kcal/mol (around 75% contribution from dispersion component, Table 5). The next most stabilized interaction pair (motif-2) forms centrosymmetric dimers in the crystal packing by using C8-H8B…N1 and C7-H7B…Cl1 hydrogen bonds (I.E = -9.058 kcal/mol). Motif-3 involves C-H…Cl (C4-H4…Cl1) hydrogen bond and C4…Cl1 short contact with I.E. = -4.924 kcal/mol, forming the third most stability contributor to the crystal structure. The stability of the crystal packing is further enhanced by weak C-H…Cl hydrogen bonds as shown in motif-4, 5 and 6.

M-2. 2, 6-Dichloro-9-(prop-2-yn-1-yl)-9H-purine

The interaction energy components calculated for 2, 6-Dichloro-9-(prop-2-yn-1-yl)-9H-purine are summarized in Table 6 and molecular interaction pairs (motif 1-5) are shown in Figure 7. In the crystal structure of the molecule, the most stable pair (motif-1, I.E = -8.867 kcal/mol) involves bifurcated hydrogen bond C4-H4…N1/Cl1, with C4-H4 acting as bifurcated donor and a hydrogen bond C4-H4…Cl1. Motif-2 comprise of π…π interaction (Cg1…Cg1/Cg2…Cg2: Cg-Cg centroid distance 3.933Å), having I.E = -7.911 kcal/mol of dispersive nature (85% contribution from dispersion energy), helps in stacking of the molecules in the crystal packing. Bifurcated hydrogen bond C6-H6B…Cl2/N3 (C6-H6B being bifurcated donor) forms motif-3 and has energy contribution of I.E = -6.286kcal/mol in the packing. The C8-H8…N2 hydrogen bonds in motif-4 is having I.E. = -4.589kcal/mol with around 51% contribution from the coulombic term (Table 6). A weak intermolecular halogen bond C2-Cl2…C8 also found in the crystal packing with I.E = -1.506 kcal/mol (motif-5).

M-3. 2-Amino-6-chloropurine

Dominant intermolecular interaction pairs (motifs) extracted from the crystal structure of *2*-Amino-6-chloropurine is presented in Figure 8. Strong N-H…N (N9-H9…N7) hydrogen bonds forming motif-1 emerges as the energetically most stable interaction pair in the packing, has I.E = -12.357 kcal/mol (around 55% coulombic contribution, Table 7). The N21-H21…N1 and N21-H22…N3 hydrogen bonds (I.E = -12.118kcal/mol with 51% coulombic contribution, motif-2) forms hydrogen bonded virtual rings with $R_2^2(8)$ graph-set motifs [37]. The π…π (Cg1…Cg1/Cg2…Cg2) interaction with I.E = -5.234kcal/mol of highly dispersive nature (around 91% dispersion component) is responsible for stacking the molecules in the crystal packing (motif-3). A C-H…N type hydrogen bond with I.E = - 2.653 kcal/mol also exist in the packing (motif-4). Weak halogen bonded interactions C6-Cl1…Cg1 (morif-5) and C6-Cl6…N9 (motif-6) with I.E. = -2.390 and -2.175 kcal/mol, respectively, provides additional stability to the crystal structure.

M-4. 2,6,8-Trichloro-9-methylpurine

Interaction energies of the most significant interactions involved in the molecular packing of 2,6,8-Trichloro-9-methylpurine are listed in Table 8 and the corresponding interaction pairs are depicted in Figure 9. The energetically most stable molecular pair (motif-1) in the crystal structure involves π...π interaction (Cg1…Cg2/Cg2…Cg1) having interaction energy I.E = -12.094 kcal/mol (around 71% contribution from dispersion energy). A halogen…π (C1-Cl1…Cg2) and a C-H…N type hydrogen bond (C6-H6…N1), constitutes the second most stable molecular pair with I.E = -12.070 kcal/mol, having 67% contribution from dispersive component (motif-2). The halogen bond C5-Cl3…N1 and a C6-H3…Cl2 hydrogen bond forming motif-3, has an energy contribution of I.E = -4.230 kcal/mol. Motif-4 (I.E. = -4.183kcal/mol) is forming virtual rings in the crystal structure with $R_2^2(8)$ graph set motif, using C5-Cl3…N1 halogen bond and C6-H1…

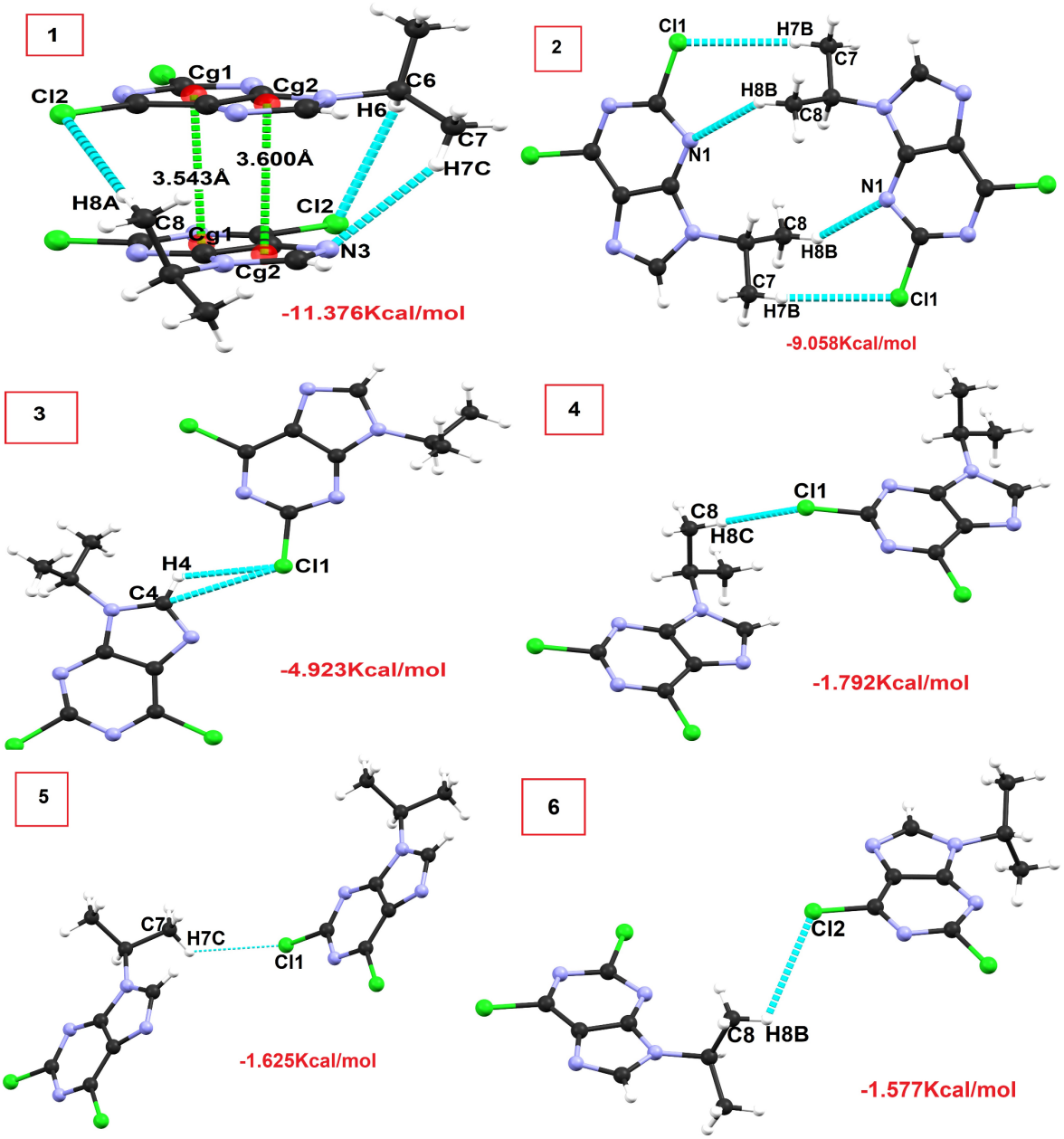

Figure 6: Intermolecular interaction pair exists in M-1.

Table 5: Intermolecular interaction energies (Kcal/mol) calculated for M-1.

Motif	Centroid Distance (Å)	E_{Cou}	E_{Pol}	E_{Dis}	E_{Rep}	E_{Tot}	Symmetry	Important Interactions
1	4.915	-3.083	-2.055	-15.822	9.560	-11.377	x,1/2-y,-1/2+z	Cg1…Cg1 Cg2…Cg2, C6-H6…Cl2 C8-H8A…Cl2 C7-H7C…N3
2	5.737	-4.278	-1.601	-7.361	4.183	-9.058	2-x,-y,2-z	C7-H7B…Cl1 C8-H8B…N1
3	9.113	-3.298	-1.219	-3.776	3.370	-4.924	-1+x,1/2-y,-1/2+z	C4-H4…Cl1 C4…Cl1
4	8.470	-0.574	-0.550	-2.223	1.554	-1.793	-1+x,y,z	C8-H8C…Cl1
5	9.708	-0.478	-0.167	-1.506	0.550	-1.625	-1+x,y,-1+z	C7-H7C…Cl1
6	9.879	-0.669	-0.143	-1.386	0.621	-1.577	2-x,-1/2+y,5/2-z	C8-H8B…Cl2

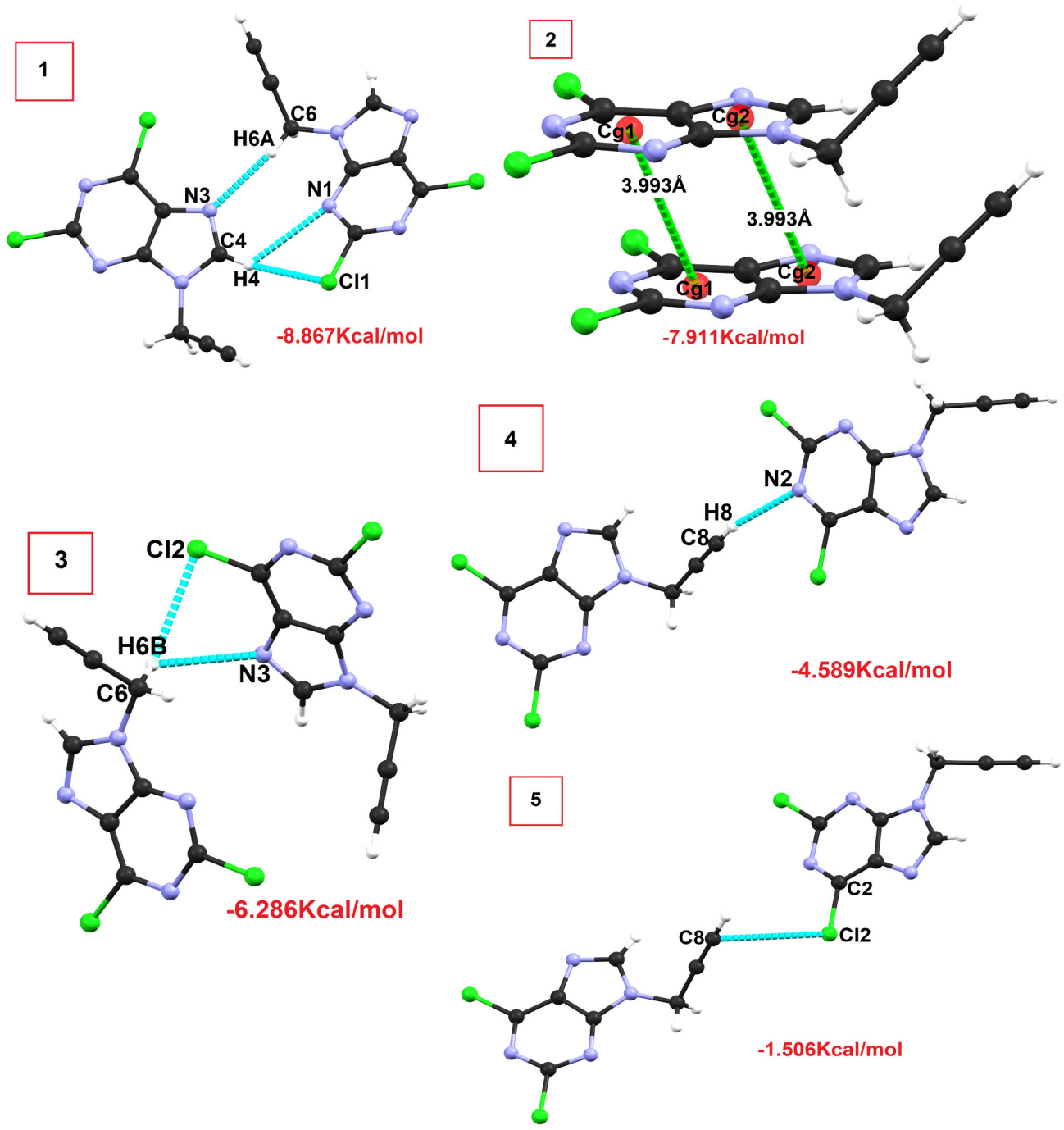

Figure 7: Intermolecular interaction pairs exist in M-2.

Table 6: Intermolecular interaction energies (Kcal/mol) exist in M-2.

Motif	Centroid Distance (Å)	E_{Cou}	E_{Pol}	E_{Dis}	E_{Rep}	E_{Tot}	Symmetry	Important Interactions
1	6.284	-6.023	-1.936	-6.166	5.234	-8.867	-1/2+x,1/2-y,1/2+z	C6-H6A…N3 C4-H4…N1 C4-H4…Cl1
2	3.993	-0.550	-1.793	-13.480	7.911	-7.911	-1+x, y,z	Cg1…Cg1 Cg2…Cg2
3	5.699	-3.059	-0.956	-4.804	2.533	-6.286	-1/2+x,1/2-y,-1/2+z	C6-H6B…Cl2/N3
4	10.704	-3.322	-0.860	-2.223	1.816	-4.589	3/2-x,-1/2+y,1/2-z	C8-H8…N2
5	10.525	-0.693	-0.167	-1.338	0.693	-1.506	½-x,-1/2+y,1/2-z	C2-Cl2….C8

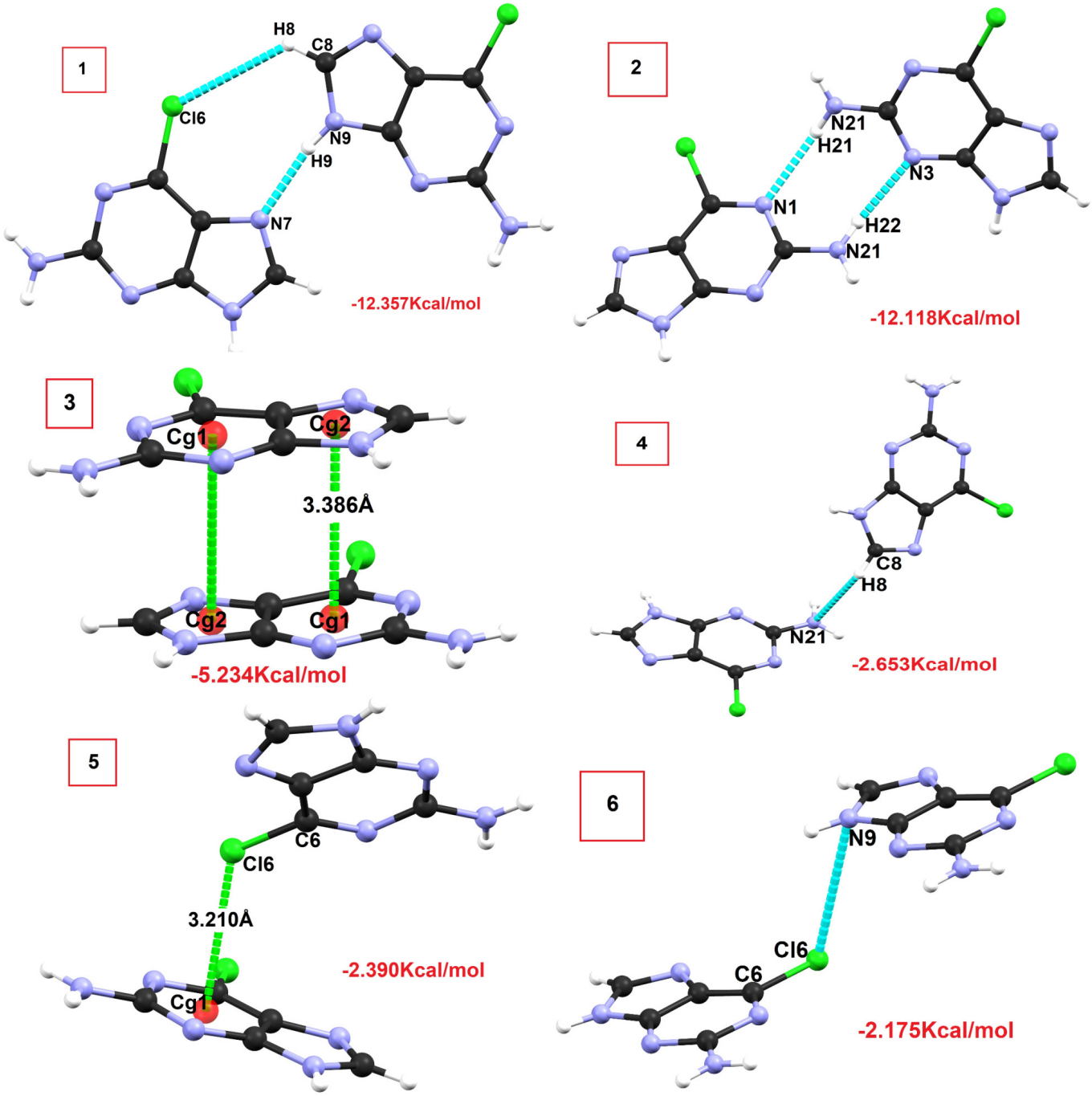

Figure 8: Intermolecular interaction pairs exist in M-3.

Table 7: Intermolecular interaction energies (Kcal/mol) exist in M-3.

Motif	Centroid Distance (Å)	E_{Cou}	E_{Pol}	E_{Dis}	E_{Rep}	E_{Tot}	Symmetry	Important Interactions
1	6.876	-14.293	-6.477	-5.306	13.719	-12.357	1+x, y,-z	N9-H9…N7
2	6.617	-13.743	-6.238	-6.955	14.818	-12.118	½-x,-1/2+y,1/4-z	N21-H21…N1 N21-H22…N3
3	3.466	0.215	-1.291	-11.592	7.433	-5.234	x,y,-z	Cg1…Cg1 Cg2…Cg2
4	7.874	-1.506	-0.311	-1.625	0.789	-2.653	½+x,1/2-y,-1/4+z	C8-H8…N21
5	5.799	-0.884	-0.860	-5.282	4.637	-2.390	3/2-x,-1/2+y, ¼-z	C-Cl…Cg1
6	7.085	-0.980	-0.430	-2.199	1.434	-2.175	x,-1+y, z	C6-Cl6…N9

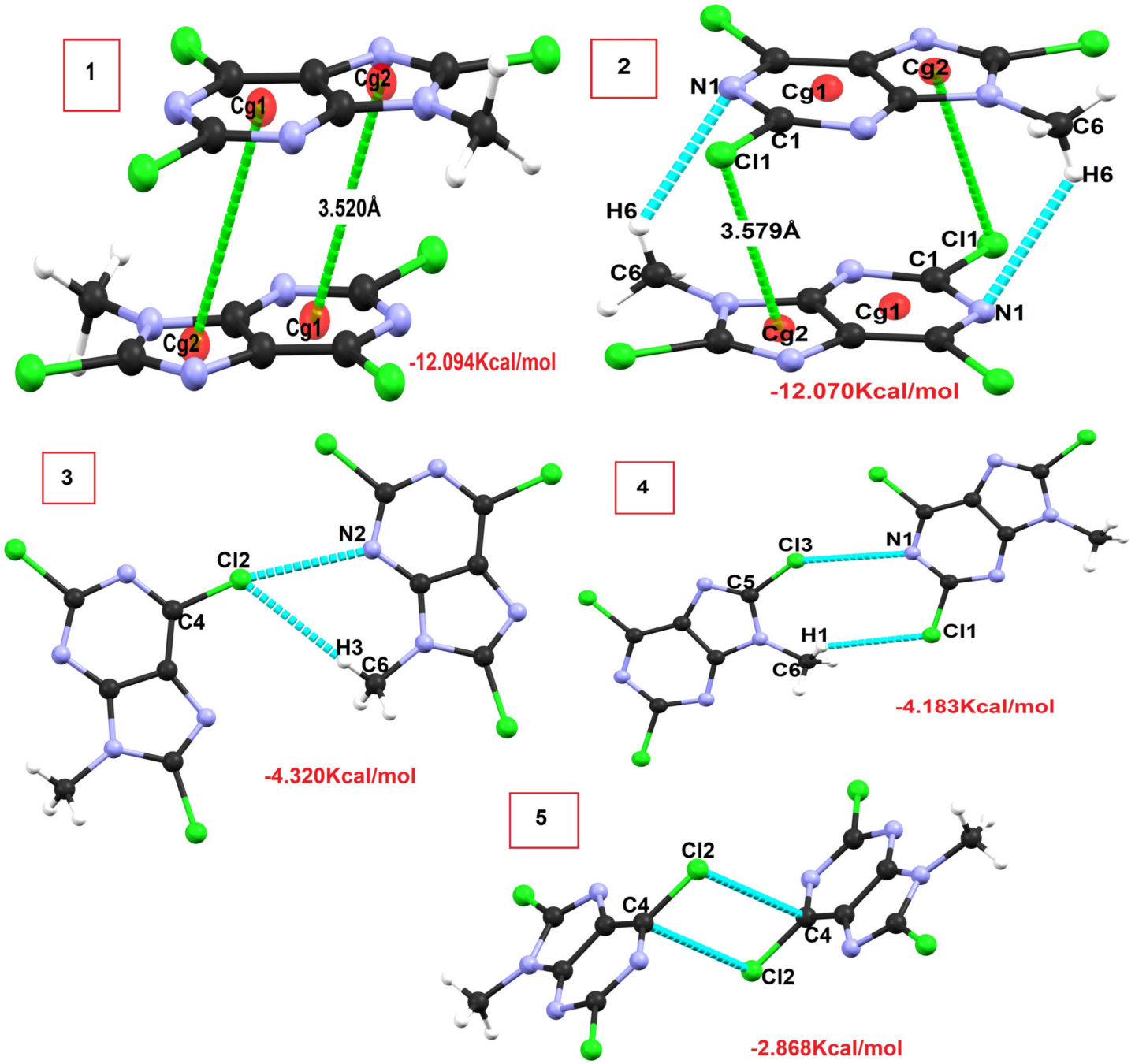

Figure 9: Intermolecular interaction pairs exist in M-4.

Table 8: Intermolecular interaction energies (Kcal/mol) exist in M-4.

Motif	Centroid Distance (Å)	E_{Cou}	E_{Pol}	E_{Dis}	E_{Rep}	E_{Tot}	Symmetry	Important Interactions
1	4.198	-4.589	-2.820	-18.523	13.838	-12.094	-x,1-y,-z	Cg1…Cg2
2	4.248	-4.780	-1.721	-13.337	7.792	-12.070	1-x,1-y,-z	C1-Cl1…Cg2 C6-H6…N1
3	7.568	-3.322	-1.291	-4.876	5.282	-4.230	x,-1+y,z	C6-H3…Cl2 C4-Cl2…N2
4	9.146	-2.079	-0.669	-3.872	2.438	-4.183	x,y,-1+z	C5-Cl3…N1 C6-H1…Cl1
5	7.646	-0.956	-0.693	-5.521	4.278	-2.868	1-x,2-y,-z	C4…Cl2

Cl1 hydrogen bond. C4…Cl2 short contact also contributes in the crystal packing with I.E. = -2.868kcal/mol (motif-5).

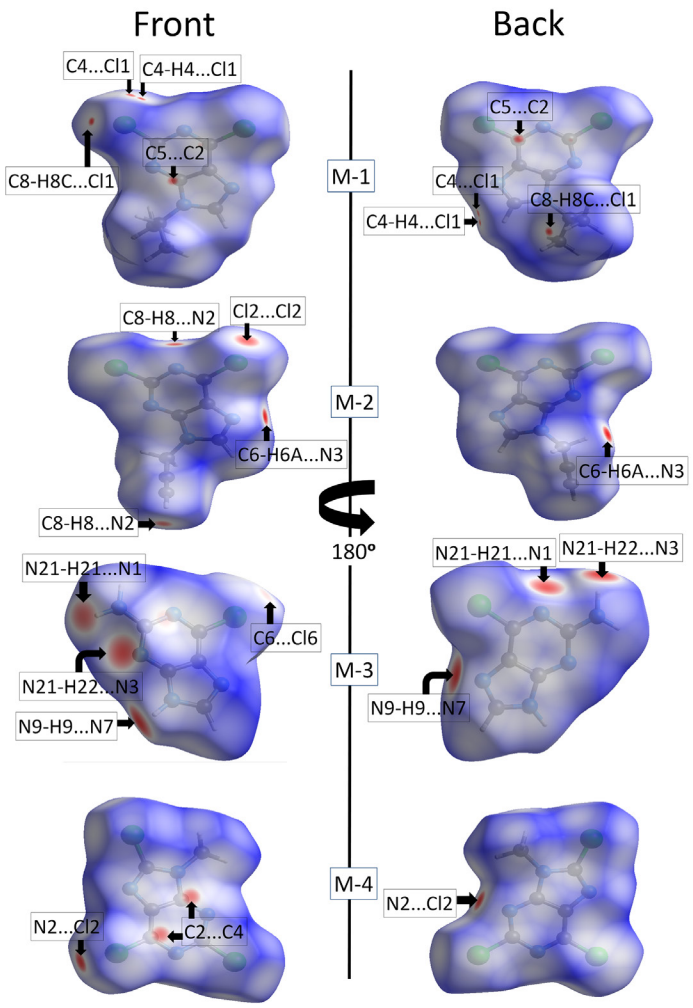

Figure 10: Comparison of Hirshfeld surfaces plotted over d_{norm} values.

Hirshfeld Surface Analysis

The presence of various intermolecular interactions involved in the crystal packing of each molecule has been studied visually by using the three-dimensional Hirshfeld surface formalism. Red regions correspond to various intermolecular short contacts exist in each structure are shown through the front and back views of d_{norm} plots (Figure 10). The size of these spots relates the strength of contacts involved [29,38]. The red spots as observed on the d_{norm} plot, for M-1, correspond to C-H…Cl, C…C and C…Cl contacts. The C-H…N and Cl…Cl interactions have been observed in case of M-2 (shown in the d_{norm} plot). The strong intermolecular N-H…N hydrogen bonds in M-3 emerge as big red spots on the d_{norm} surface and in case of M-4, these spots correspond to C…C stacking interactions and the weak C…N short contacts.

Characteristic features of the inter-contacts on the Hirshfeld surface can be represented on 2D-fingerprint plots. The hydrogen bonded interactions will emerge as spikes in the fingerprint plots and, the sharpness of the peak and d_i+d_e value depicts their relative strength, whereas the planar stacking resulted by π…π interactions would be seen as bright reddish-yellowish region in the plot [35,39]. The sharp spikes ($d_i+d_e \sim 2.0$Å) observed for N…H contact (with 35.1% contribution) in case of M-3 corresponds to the strong intermolecular N-H…N hydrogen bond and in case of M-2, spikes with $d_i+d_e \sim 2.4$Å, corresponds to C-H…N hydrogen bonds (Figure 11). The fingerprint plot analysis indicates that the highest contribution to the Hirshfeld surface comes from the Cl…H/H…Cl contacts in case of M-1 and M-4, while the N…H/H…N contacts contribution is maximum in case of M-2 and M-3. The Cl…H/H…Cl contact in M-2 and M-3 has second highest contribution to the Hirshfeld surface. Overall, the Cl involving short contacts shows significant contribution towards Hirshfeld surface, in all the structures. Halogen-halogen contact (Cl…Cl) has sizeable contribution in case of M-2 and M-4 (8.8% and 14.0%, respectively).

On the shape index plot (Figure 12), pairs of blue and red color patches, represents the location where two molecule's Hirshfeld surfaces interlock each other. The shape index characteristic relies on the surface's local curvature and is particularly effective for detecting planar stacking patterns [40]. The complementary blue and red triangles in the shape index plots show the existence of π…π stacking interactions and such regions are enclosed by red rectangular boxes (Figure 12). The root-mean-square of the curvature of molecule's surface is used for defining the curvedness plot [29]. Characteristics of planar stacking of molecules in the crystal packing can be seen as flat patches on the curvedness plot (Figure 13).

Conclusions

The B3LYP/6311+G(d,p) optimized molecular geometry of the chloro-purine structures correlate well with the corresponding experimental X-ray structures. HOMO-LUMO energy analysis found that structures of M-1 and M-2 are chemically most stable amongst the four. The lattice energy calculated by PIXEL procedure shows that, the combine effect of all the interactions in the crystal structures of M-1, M-2 and M-4 are dispersive in nature, while in case of M-3, it is dominated by the coulombic term. Intermolecular hydrogen bonds of the type C-H…N and C-H…Cl, and the π…π (interaction energy of -5 to -12kcal/mol), plays major role in the packing stability of the M-1, M-2 and M-4. In M-3, the packing stability is mainly derived by strong N-H…N hydrogen bonds having energy of -12 to -12.5kcal/mol. Other weak interactions such as C-Cl…π, C-Cl…N, also exist in the molecular packing of these structures with energy contribution in the range -1 to -5kcal/mol. Strong and weak intermolecular short contacts have also been visually identified on the Hirshfeld surface of each molecule. The major contributors to the Hirshfeld surface of the structures are from Cl...H, N…Cl, N…C, N...H and H…H short contacts. The π…π stacking interaction is also observed in all the structures and is confirmed by the shape index and curvedness plots. The PIXEL energies and the Hirshfeld surface analysis carried out on the structures shows that, Cl-involving interactions are weak in nature, but have prominent role in the crystal packing of these compounds.

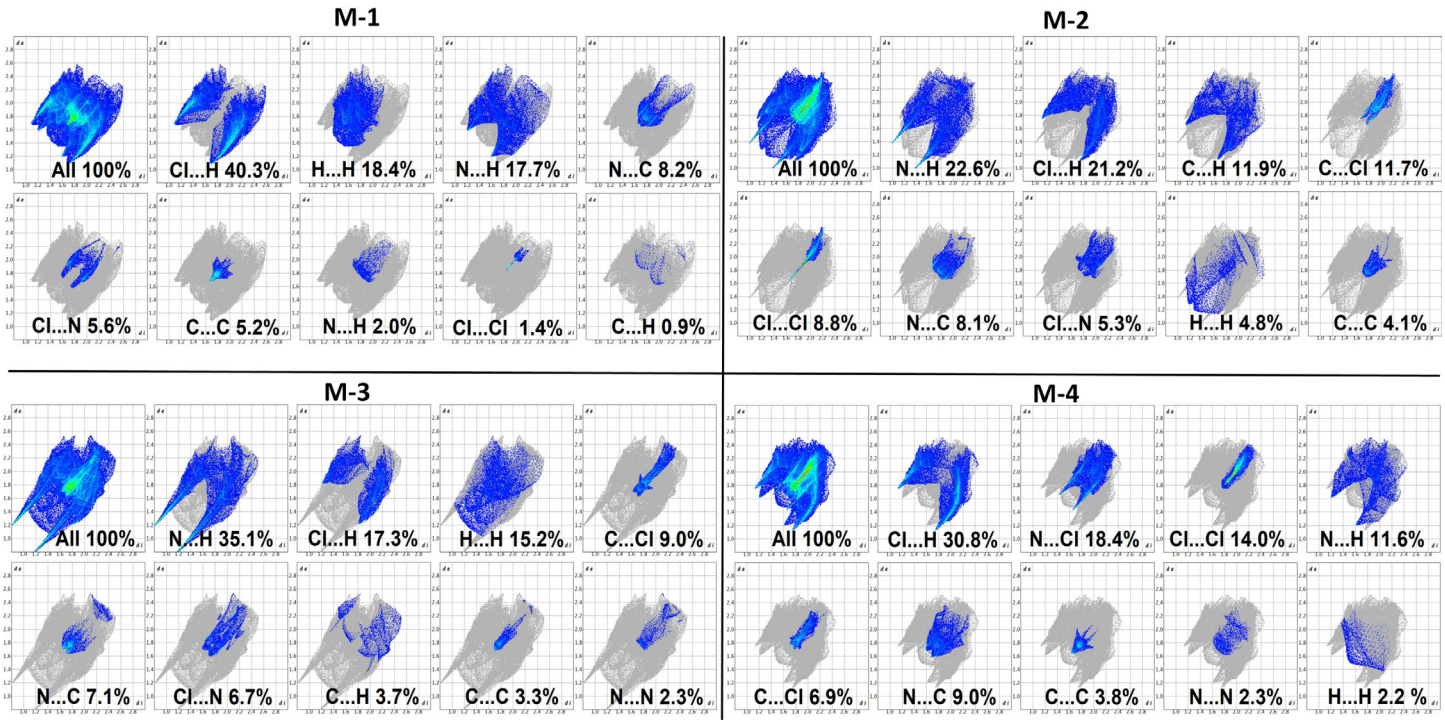

Figure 11: Comparison of 2D-fingerprint plots.

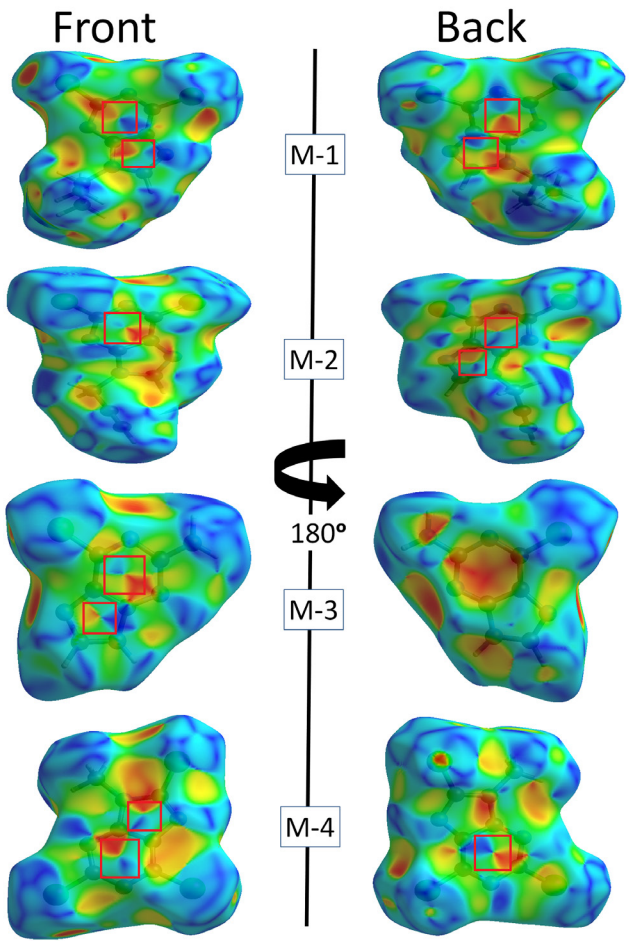

Figure 12: Shape index plots comparison of the molecules.

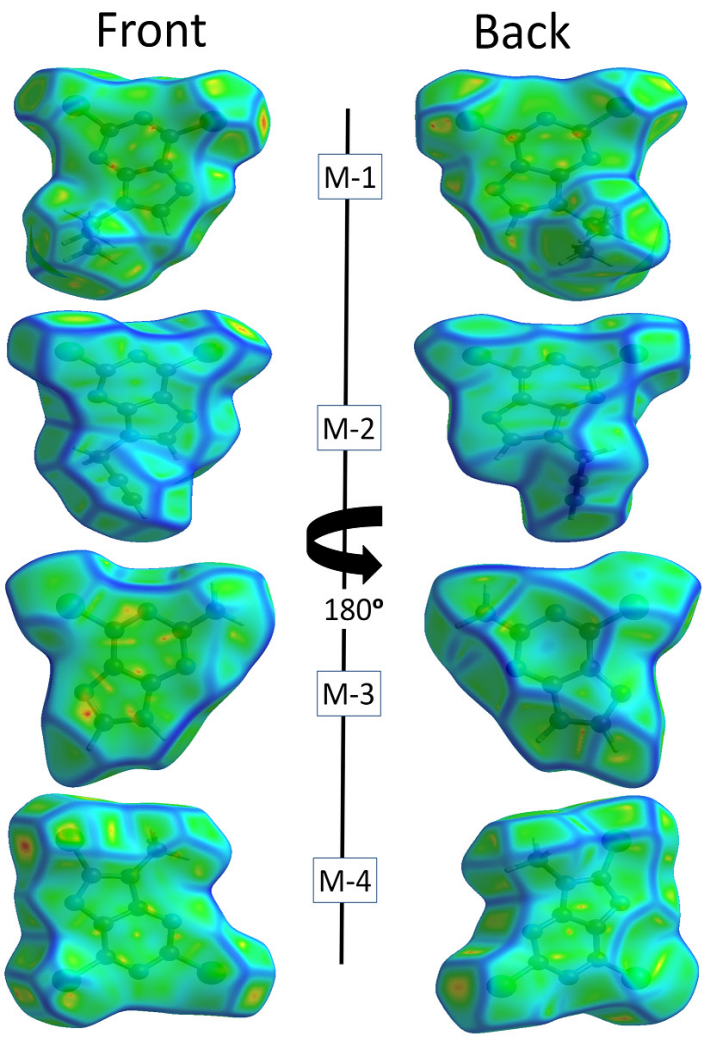

Figure 13: Curvedness plots comparison of the molecules.

Acknowledgement

Rajni Kant acknowledges the financial support received from the University of Jammu for the licensed access of CSD and for some funds under RUSA 2.0 project.

References

1. Lang DK, Kaur R, Arora R, et al. Nitrogen-Containing Heterocycles as Anticancer Agents: An Overview. Anticancer Agents Med Chem. 2020; 20: 2150-2168.
2. Le Doan T, Perrouault L, Praseuth D, et al. Sequence-specific recognition, photocrosslinking and cleavage of the DNA double helix by an oligo-(α]-thymidylate covalently linked to an azidoproflavine derivative. Nucleic Acids Res. 1987; 15: 7749-7760.
3. Meijer L, Raymond E. Roscovitine and other purines as kinase inhibitors. From starfish oocytes to clinical trials. Acc Chem Res. 2003; 36: 417-425.
4. Sharma S, Singh J, Ojha R, et al. Design strategies, structure activity relationship and mechanistic insights for purines as kinase inhibitors. Eur J Med Chem. 2016; 112: 298-346.
5. Bonnet PA, Robins RK. Modulation of leukocyte genetic expression by novel purine nucleoside analogues. A new approach to antitumor and antiviral agents. J Med Chem. 1993; 36: 635-653.
6. Nair V, Bera B, Kern ER. Synthesis and biological activities of 2-functionalized purine nucleosides. Nucleosides Nucleotides Nucleic Acids. 2003; 22: 115-127.
7. Conejo-Garcia A, Cruz-Lopez O, Gomez-Perez V, et al. Synthesis of Purine Derivatives as Scaffolds for a Diversity of Biological Activities. Curr Org Chem. 2010; 14: 2463-2482.
8. Legraverend M. Recent advances in the synthesis of purine derivatives and their precursors. Tetrahedron. 2008; 64: 8585-8603.
9. Joshi B V, Jacobson KA. Purine derivatives as ligands for A3 adenosine receptors. Curr Top Med Chem. 2005; 5: 1275-1295.
10. Dinesh S, Shikha G, Bhavana G, et al. Journal of Pharmaceutical and Scientific Innovation Biological activities of purine analogues: a review. 2012; 1: 29-34.
11. Krasnov VP, Levit GL, Musiyak VV, et al. Fragment-based approach to novel bioactive purine derivatives. Pure Appl Chem. 2020; 92: 1277-1295.
12. Zheng H, Hou J, Zimmerman MD, et al. The future of crystallography in drug discovery. Expert Opin Drug Discov. 2014; 9: 125-137.
13. van Mourik T, Bühl M, Gaigeot M-P. Density functional theory across chemistry, physics and biology. Philos Trans R Soc A Math Phys Eng Sci. 2014; 372: 20120488.
14. Bochevarov AD, Watson MA, Greenwood JR, et al. Multiconformation, Density Functional Theory-Based pKa Prediction in Application to Large, Flexible Organic Molecules with Diverse Functional Groups. J Chem Theory Comput. 2016; 12: 6001-6019.
15. Kerru N, Gummidi L, Bhaskaruni SVHS, et al. A comparison between observed and DFT calculations on structure of 5-(4-chlorophenyl)-2-amino-1,3, 4-thiadiazole. Sci Rep. 2019; 9: 19280.
16. Cheng G-J, Zhang X, Chung LW, et al. Computational Organic Chemistry: Bridging Theory and Experiment in Establishing the Mechanisms of Chemical Reactions. J Am Chem Soc. 2015; 137: 1706-1725.
17. Lu W, Sengupta S, Petersen JL, et al. Mitsunobu Coupling of Nucleobases and Alcohols : An Efficient , Practical Synthesis for Novel Nonsugar Carbon Nucleosides. J Org Chem. 2007; 72: 5012-5015.
18. Lynch DE, McClenaghan I. Three 2-aminopurine derivatives. Acta Crystallogr Sect C Cryst Struct Commun. 2003; 59: 53-56.
19. Xu K, Ho DM, Pascal RA. Azaaromatic Chlorides: A Prescription for Crystal Structures with Extensive Nitrogen-Chlorine Donor-Acceptor Interactions. J Am Chem Soc. 1994; 116: 105-110.

20. Baseden KA, Tye JW. Introduction to Density Functional Theory: Calculations by Hand on the Helium Atom. J Chem Educ. 2014; 91: 2116-2123.
21. Frisch MJ, Trucks GW, Schlegel HB, et al. Gaussian 09; Gaussian, Inc. Wallingford, CT, 2009; 32: 5648-5652.
22. Becke AD. Density-functional thermochemistry. III. The role of exact exchange. J Chem Phys. 1993; 98: 5648-5652.
23. Lee C, Yang W, Parr RG. Development of the Colle-Salvetti correlation-energy formula into a functional of the electron density. Phys Rev B. 1988; 37: 785-789.
24. Dennington R, Keith TA, Millam JM. GaussView Version 6.0.16. 2016.
25. Gavezzotti A. Calculation of lattice energies of organic crystals: the PIXEL integration method in comparison with more traditional methods. Zeitschrift für Krist - Cryst Mater. 2005; 220: 499-510.
26. Gavezzotti A. Equilibrium structure and dynamics of organic crystals by Monte Carlo simulation: critical assessment of force fields and comparison with static packing analysis. New J Chem. 2013; 37: 2110-2119.
27. Gavezzotti A. Efficient computer modeling of organic materials. The atom–atom, Coulomb–London–Pauli (AA-CLP) model for intermolecular electrostatic-polarization, dispersion and repulsion energies. New J Chem. 2011; 35: 1360-1368.
28. McKinnon JJ, Spackman MA, Mitchell AS. Novel tools for visualizing and exploring intermol{\-}ecular interactions in molecular crystals. Acta Crystallogr Sect B. 2004; 60: 627-668.
29. Spackman MA, Jayatilaka D. Hirshfeld surface analysis. CrystEngComm. 2009; 11: 19-32.
30. Spackman PR, Turner MJ, McKinnon JJ, et al. {\it CrystalExplorer}: a program for Hirshfeld surface analysis, visualization and quantitative analysis of molecular crystals. J Appl Crystallogr. 2021; 54: 1006-1011.
31. Fukui K, Yonezawa T, Shingu H. A Molecular Orbital Theory of Reactivity in Aromatic Hydrocarbons. J Chem Phys. 1952; 20: 722-725.
32. Jalbout AF, Trzaskowski B, Hameed AJ. Theoretical investigation of the electronic structure of 1-(3,4; 3,5 and 3,6-bis-selenocyanato-phenyl) pyrrolidinofullerenes. J Organomet Chem. 2006; 691: 4589-4594.
33. Li H, Zhang Z, Liu Y, et al. Functional Group Effects on the HOMO–LUMO Gap of g-C3N4. Nanomaterials. 2018; 8: 589.
34. Sakthivel S, Alagesan T, Muthu S, et al. Quantum mechanical, spectroscopic study (FT-IR and FT - Raman), NBO analysis, HOMO-LUMO, first order hyperpolarizability and docking studies of a non-steroidal anti-inflammatory compound. J Mol Struct. 2018; 1156: 645-656.
35. Singh M, Murugavel S, Chandrasekaran R, et al. Quantum, Hirshfeld surface, crystal voids, energy framework and molecular docking analysis of two halogen-containing benzimidazole-2-thione structures. Mol Cryst Liq Cryst. 2022; 0: 1-15.
36. Brahmia A, Bejaoui L, Rolicek J, et al. Synthesis, crystal structure, Hirshfeld surface analysis and DFT calculations of 2, 2, 2-tribromo-1-(3,5-dibromo-2-hydroxyphenyl)ethanone. J Mol Struct. 2022; 1248. 131313.
37. Bernstein J, Davis RE, Shimoni L, Chang N-L. Patterns in Hydrogen Bonding: Functionality and Graph Set Analysis in Crystals. Angew Chemie Int Ed English. 1995; 34: 1555-1573.
38. McKinnon JJ, Jayatilaka D, Spackman MA. Towards quantitative analysis of intermolecular interactions with Hirshfeld surfaces. Chem Commun. 2007; (37):3814-3816.
39. Spackman MA. Molecules in crystals. Phys Scr. 2013; 87: 48103.
40. Ahmed MN, Madni M, Anjum S, et al. Crystal engineering with pyrazolyl-thiazole derivatives: structure-directing role of π-stacking and σ-hole interactions. CrystEngComm. 2021; 23: 3276-3287.